eISSN 1303-1775 • pISSN 1303-1783

Neuroanatomy (2008) 7: 83–92

Original Article

Multimodal MRI evaluation of acute mild-contusive injury in mouse spinal cord

Published online 17 December, 2008 © http://www.neuroanatomy.org

Peter Cheng-te CHOU
Ilkan TATAR
Mehmet BILGEN ✦

Radiology and Radiological Science, Medical University of South Carolina, 169 Ashley Avenue, Charleston, SC 29425, USA.

✦ Mehmet Bilgen, Ph.D.
169 Ashley Avenue
Medical University of South Carolina
Charleston, SC 29425, USA.
☎ +1 843-792-8171
+1 843-792-2642
✉ bilgen@musc.edu

Received 15 February 2008; accepted 24 April 2008

ABSTRACT

In vivo preclinical imaging of spinal cord injury (SCI) in rodent models is sought after for obtaining clinically relevant neuropatholocial information in translational research. This paper uses multimodal magnetic resonance imaging (MRI) to investigate spinal cords that were injured mildly at the thoracic T11 level in six C57BL/6 female mice. On postinjury days 1 and 3, the mice were subjected to neurobehavioral evaluations proceeded by high resolution MRI scans. The MRI protocols included proton density weighted, T2-weighted and diffusion tensor imaging. The scans on day 3, the injured cords were evaluated using postmortem histological analysis. The neurobehavioral tests indicated that injured mouse developed functional deficits in hindlimbs that worsen slowly from day 1 to day 3. Microanatomical images from these days depicted slight variations in the intensity patterns within the injured SC parenchyma. These changes suggested gradually progressive neuropathology. The quantitative diffusion tensor measurements showed steady deterioration of the neurostructure, prominently in the dorsal region which received the mechanical impact. The injured cords examined with different stains depicted gross tissue morphology that matched the anatomical images and allowed interpreting the neurostructural data. At the injury site, changes in the grey and white matters and neuronal cell swelling were evident and supported the diffusion measurements, but the fibrotic tissue deposition was minimal. The results together demonstrated the value of evaluating injured mouse SC using in vivo MRI and how this may potentially play an important role in characterizing the efficacy of a therapeutic strategy aimed at improving the outcome from SCI. © **Neuroanatomy. 2008; 7: 83–92.**

Key words [spinal cord] [spinal cord injury] [mouse] [preclinical] [translational] [acute] [magnetic resonance imaging] [diffusion] [diffusion tensor imaging]

Introduction

The availability of diverse strains and transgenic varieties makes mouse an appealing animal model in experimental spinal cord injury (SCI) studies [1-4]. Using these models, neuroscience research is focused on understanding the biological basis and mechanisms of pathobiology and injury characteristics in different strains of mice [5-7]. Although, mouse offers novel possibilities, it also exhibits an injured spinal cord (SC) neuropathology unseen in human or rat. In particular, the inflammatory response produces lesions with dense fibrous connective tissue, similar to those in wound-healing or scarring [8,9].

Although, the primary damage from mechanical insult is unavoidable, the postinjury response and secondary pathobiological activities in injured SC can potentially be manipulated using interventions aimed at improving neuroprotection, repair and recovery from the injury. Such efforts are likely to yield effective countermeasures with capabilities to minimize the pathobiological and neurofunctional consequences of the SCI. The degree of initial mechanical damage and subsequent secondary events following experimental SCI in mouse are traditionally evaluated using postmortem tissue analysis based on histology and immunohistochemistry. We suggest that the research can further benefit from the existing in vivo neuroimaging methods, if integrated properly to image the injured mouse SC. In particular, a variety of magnetic resonance imaging (MRI) modalities can provide anatomical, structural and functional information about injured mouse SC. Towards this purpose, we and others are investigating such translational opportunities [10-18]. The feasibility and merits of anatomical MRI to evaluate lesion development longitudinally were demonstrated recently [19]. But, comprehensive and noninvasive data obtained from this particular study also revealed that the contused mouse SC exhibits unique MR signal patterns, previously unfamiliar in rats and humans. In particular, fibrotic tissue appears hypointense on the images. In addition, past studies based on postmortem tissue analysis suggested that the first 72 hours (3 days) of the SCI is the most critical time period and offers a window of opportunity for treatments applied within this time frame [20-23]. For developing effective therapeutic strategies in experimental studies with mouse strains, it is also paramount to employ a SCI model that sensitively responds to the treatment at the acute phase of the injury and is also capable of producing measurable neuropathological and behavioral changes. Therefore, this paper investigates mildly injured SC in mouse and presents results from neuropathological evaluations with multimodal MRI as well as histological analysis and neurobehavioral assessments in the acute phase (postinjury day 1 and 3) of the SCI.

Materials and Methods

All experiments were carried out with twelve-week old female C57BL/6 mice (n=6) in accordance with a protocol approved by the Institutional Animal Care and Use Committee. Below, we identify the mice used in the

Figure 1. In vivo proton-density axial image of a normal mouse spinal cord at the thoracic T11 level.

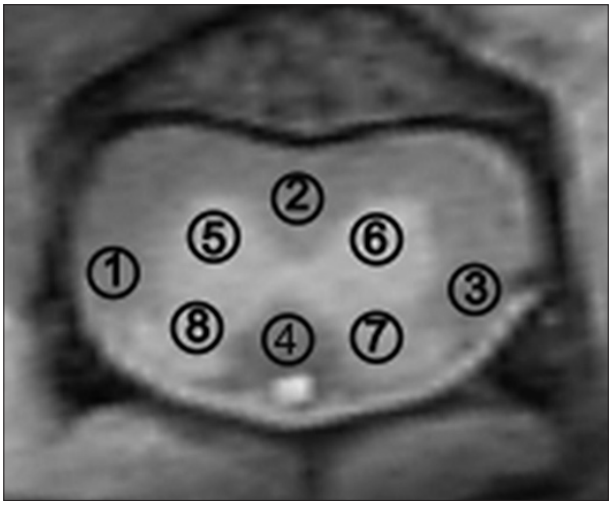

Figure 2. Regions of interests selected to measure principal diffusivities and fractional anisotropy index within white matter (***circles 1-4***) and grey matter (***circles 5-8***). The spatial locations of the ROIs are drawn on a background anatomical image of normal mouse spinal cord in Figure 1.

studies with labels M1 through M6. All of the mice M1-M6 were subjected to SCI and participated in the MRI scans on postinjury days 1 and 3 and the lesions were analyzed using postmortem histology.

Procedures for surgeries and spinal cord injury

All surgeries were performed in sterile conditions. The mouse was initially anesthetized by a spontaneous inhalation of 4% isoflurane in an induction chamber and then moved to a surgery mat. The anesthesia level was reduced to 1.5% isoflurane delivered in a mixture of 40% oxygen and 58% air through a nose mask during the surgeries. If needed further adjustments in fine amounts were made on the percentage of the isoflurane level. The surgical procedures involved a midline incision posteriori from the thoracic levels T10 to T12, followed by dissection of the bilateral vertebral muscles to expose the dorsal laminae and spinous processes. Laminectomy was performed at the T11 level to expose the SC by exercising a special care not to damage the dura mater. The spinous processes at T10 and T12 adjacent to the laminectomy were stabilized using two hemostatic forceps attached to the injury device [24]. A 1-mm diameter injury bit was positioned perpendicular to the dorsal surface of SC and the cord was injured using parameters: impact velocity of 0.75 m/s; surface displacement depth of 0.3 mm; and compression duration of 85 ms. After the injury, the overlying muscle layers were sutured and the skin was closed tightly. Then, the injured mouse was left to recover in a heated cage and received postoperative care.

MRI scans

Each injured mouse was scanned on days 1 and 3 using a 9.4-T horizontal INOVA Varian system (Varian, Palo Alto, CA) and an inductively coupled surface coil [25]. The scan was performed when the mouse was under a general anesthesia with a mixture of 1.5% isoflurane, 40% oxygen and 58% air delivered in through a nose mask. Vital signs (respiration, heart rate and body temperature) of the anesthetized animal were monitored using a MRI-compatible monitoring and gating system (Model 1025, SA Instruments Inc., Stony Brook, NY). Respiratory-gated acquisition was used to increase the image quality by minimizing the breathing related image artifacts whenever necessary.

High-resolution anatomical images were acquired in sagittal and axial views using a spin-echo sequence in multislice and interleaved fashion. The scan parameters

Figure 3. An excised mouse spinal cord. Arrow points to the site of the injury. Color version is available online.

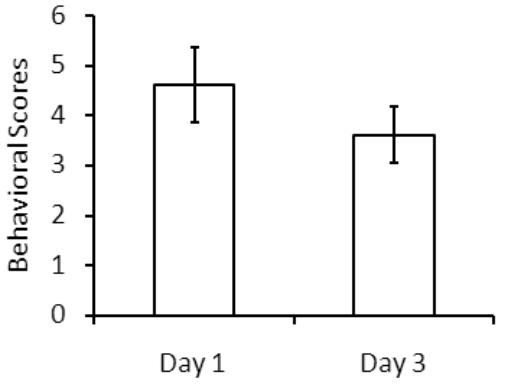

Figure 4. Locomotion performance of injured mice measured at two time points using Basso mouse scale (n = 6, mean ± std).

for the sagittal images were TR/TE = 2500/12 ms, field-of-view (FOV) = 26 X 8 mm^2, matrix = 256 X 128, in-plane pixel resolution = 100 X 63 μm, slice thickness = 0.5 mm, number of experiments (NEX) = 2. The corresponding parameters for the axial images were TR/TE = 2500/12 ms, FOV = 12 X 8 mm^2, matrix = 128 X 128, in-plane pixel resolution = 94 X 63 μm, slice thickness = 1 mm; NEX = 2. These data constituted proton density (PD) images. A typical axial PD image acquired with these parameters from a normal cord at the T11 level is provided in Figure 1 to serve as a reference. The intensity contrast on this normal cord image clearly delineates the gross anatomical details of the cord within the white matter (WM) and grey matter (GM) as well as the surrounding spinal structures. The MRI infrastructure currently in place in our laboratory allows achieving high level of quality in imaging the mouse SC on a routine basis.

For microstructural imaging, diffusion weighted images were acquired using diffusion gradient strength = 80 mT/m, width (δ) = 6.5 ms and separation (Δ) = 11 ms to produce a b-value of 534 s/mm^2. The imaging parameters for these scans were TR/TE = 2000/26 ms, FOV = 12 X 8 mm^2, image matrix = 128 X 128, in-plane pixel resolution = 94 X 63 μm, slice thickness = 1 mm and NEX = 2 [12,25,26]. The baseline data acquired in the absence of the diffusion weighting constituted the T2-weighted images.

MRI data analysis

The acquired MRI data were analyzed using the scanner's control software VMRJ (Varian, Palo Alto, CA). The diffusion-weighted images were processed to estimate the elements of diffusion tensor (DT), statistically representing the motion of water molecules in each image voxel, and subsequently its three eigenvalues (λ_1, λ_2 and λ_3) and fractional anisotropy (FA) index [12,27,28]. The eigenvectors describe the principal diffusivities of water molecules along the three orthogonal directions of DT in a given voxel. The FA index is a scalar rotationally invariant quantity expressed as a function of eigenvalues. This index is commonly used to characterize the degree of anisotropy in diffusion properties of the underlying tissue within the voxel. Once the eigenvalues and FA values were computed for each voxel throughout the injured cord, the results were combined to form two dimensional maps on the slice corresponding to the injury epicenter. To examine the regional differences on these maps, we selected eight regions of interests (ROIs) distributed symmetrically within the parenchyma of the SC. The positioning and number assignments of the selected regions are shown in Figure 2. For the GM, we chose four ROIs localized in two anterior and two dorsal horns of the cord. For the WM, we selected four ROIs - two in the lateral, one in the ventral and one in the dorsal funiculus. The measurements from all voxels within a selected ROI were averaged and the resulting mean value was recorded as measurement for that particular region. At the end of the analysis, each mouse had a

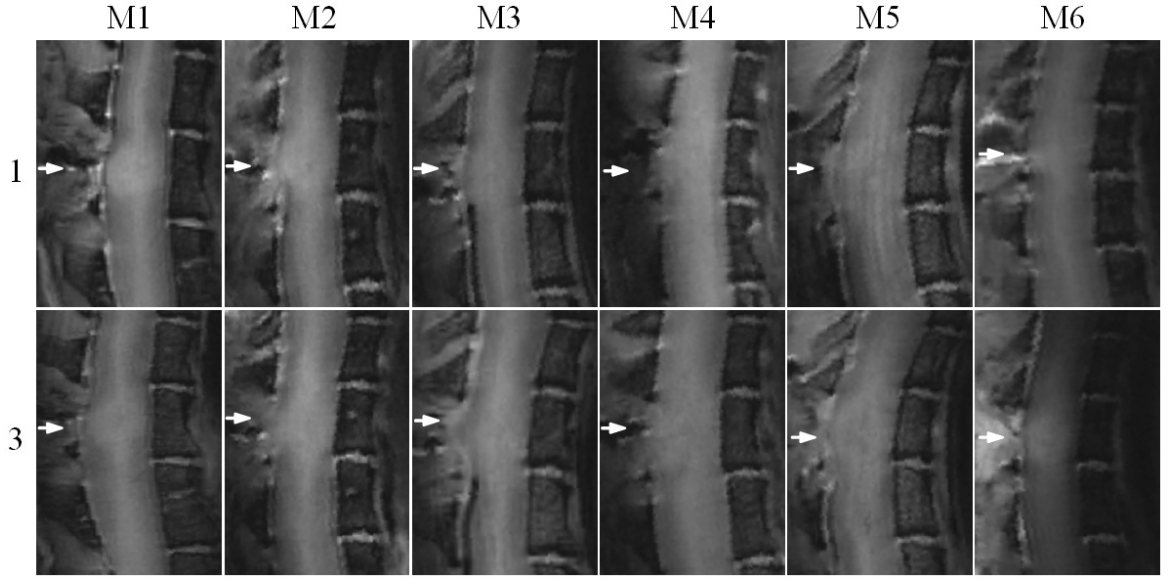

Figure 5. Sagittal proton density images of six mice with injured spinal cord on days 1 and 3. The ***arrows*** point to the site of the injury.

total of 16 measurements - 8 on day 1 and 8 on day 3, for each of the parameters λ_1, λ_2, λ_3 and FA. From the measurements of λ_2, λ_3 parameters, we have calculated $\lambda\perp$ using the following formula: $\lambda\perp = (\lambda_2+\lambda_3)/2$. All these measurements were combined in a table. To be consistent with the nomenclature used in the previous reports, we denoted $\lambda_1 = \lambda_{||}$ as an expression of longitudinal diffusivity of water molecules along the axonal fibers, and $\lambda\perp$ as an expression of transverse diffusivity combining molecular motion perpendicular to the direction of fibers.

Neurobehavioral evaluation

Each mouse was evaluated for neurological deficits in its behavioral function using Basso Mouse Scale (BMS) [7]. This new scale was designed to rate the open field locomotion specifically for injured mouse. Prior to the MRI scans on days 1 and 3, two observers independently assessed the animal's performance and assigned a score between 1 and 9 to reflect the observed neurobehavioral deficits. The two scores by the observers were averaged to obtain a final score.

Postmortem tissue analysis

Following the MRI scan on day 3, mouse was euthanized by intracardiac perfusion with 50 mL of phosphate buffered saline (PBS) solution, followed by 50 mL of 4% formaldehyde PBS solution that were delivered through a 23-gauge needle connected to a perfusion pump. The SC was excised and fixed in 4% formaldehyde. Figure 3 shows a picture of an excised mouse SC with an injury at the T11 level. This sample is fixed in formalin and the area colored in brown on the cord indicates the site of injury. After evaluating axial and sagittal MRI data from each mouse carefully, a decision was made whether to section the sample in transverse or longitudinal plane. Accordingly, the sample was embedded in paraffin and cut in 10 μm thick serial sections for mounting on slides. The slides were then stained with hematoxylin and eosin (H&E), Picrosirius red (PSR), or Luxol fast blue (LFB), and viewed with a microscope at 4X, 20X or 40X magnification and digital images were acquired with a camera attached to the microscope. The stained samples were evaluated for gross tissue morphology, residual WM and GM, neuropathology, collagen deposition, connective tissue and matrix composition at or near the site of lesion.

Statistical analysis

The statistical analysis was performed on $\lambda_{||}$, $\lambda\perp$ and FA values for each region shown in Figure 2 and mean BMS-based scores from all animals. The mean BMS scores

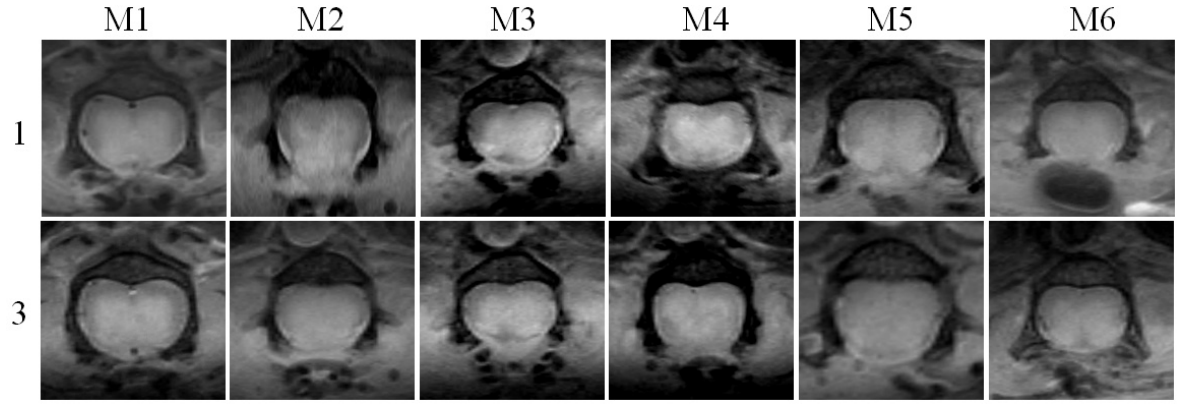

Figure 6. Axial proton density images of six mice with injured spinal cords on days 1 and 3. In all cases, the laminectomy is seen at the dorsal (towards the bottom of the image) aspect of the cord. The altered "butterfly" shaped GM intensity denotes the loss of GM/WM contrast. The central zone of spinal cord is seen with most damage, in comparison with almost spared periphery. The signal pattern on day 3 became more inhomogenous, suggesting further damage.

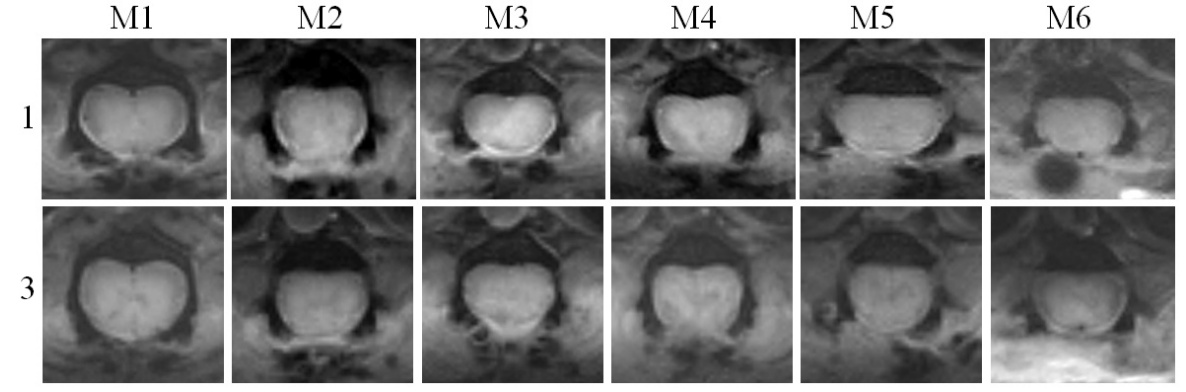

Figure 7. Axial T2-weighted images of six mice with injured spinal cords on postinjury days 1 and 3.

gathered from each animal were listed in two groups as day 1 and day 3, and compared using paired Student's t test. Statistical significance was defined at $P<0.05$. The data gathered from all animals for each DTI parameter on day 1 or day 3 were grouped together and mean and standard deviation values were computed.

Results

All of the mice participated in the experiments have tolerated the surgical procedures and injuries as well as prolonged anesthesia during the MRI scans. The injury protocol resulted in pathologically mild injuries, but with measurable behavioral deficits on postinjury days 1 and 3. The overall neurological performance of the participating animals is displayed in Figure 4, where behavioral assessments scored according to the BMS before the MRI scans were plotted against the days.

During preparation for scan, each mouse was carefully placed supine over an inductively coupled radio frequency

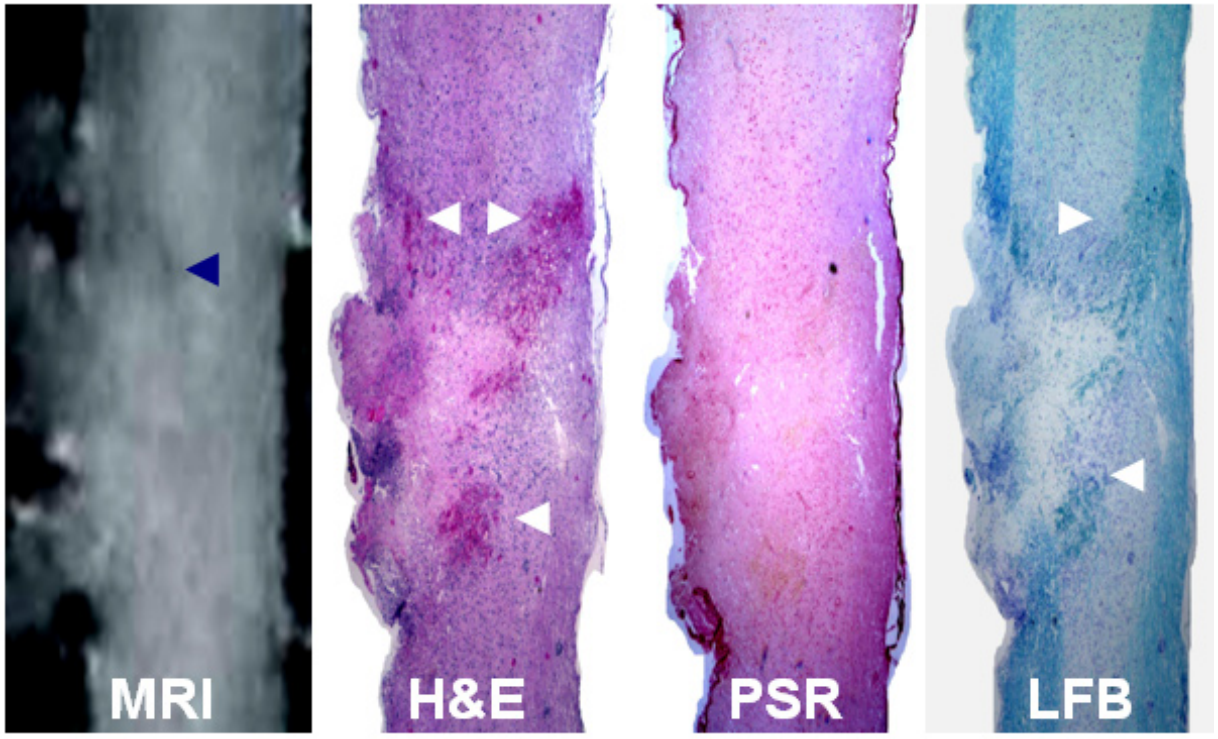

Figure 8. Comparison of the sagittal MRI of the mouse M4 on day 3 with the corresponding H&E, PSR and LFB stained histology images. Color version is available online.

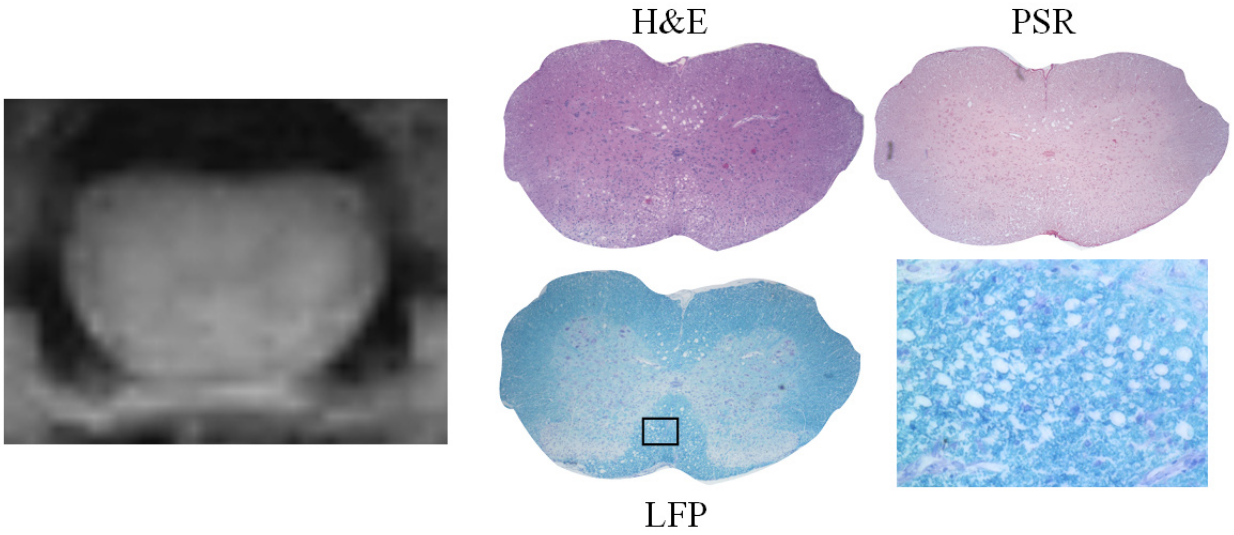

Figure 9. Comparison of the axial MRI of mouse M2 on day 3 with the corresponding H&E, PSR and LFB stained histology images. The H&E strained slide depicts microhemorrhages in the GM. PSR staining indicates lack of fibrotic tissue deposition. The LFP stain shows normal appearing GM and WM, but with neuronal cell swelling in some areas. Color version is available online.

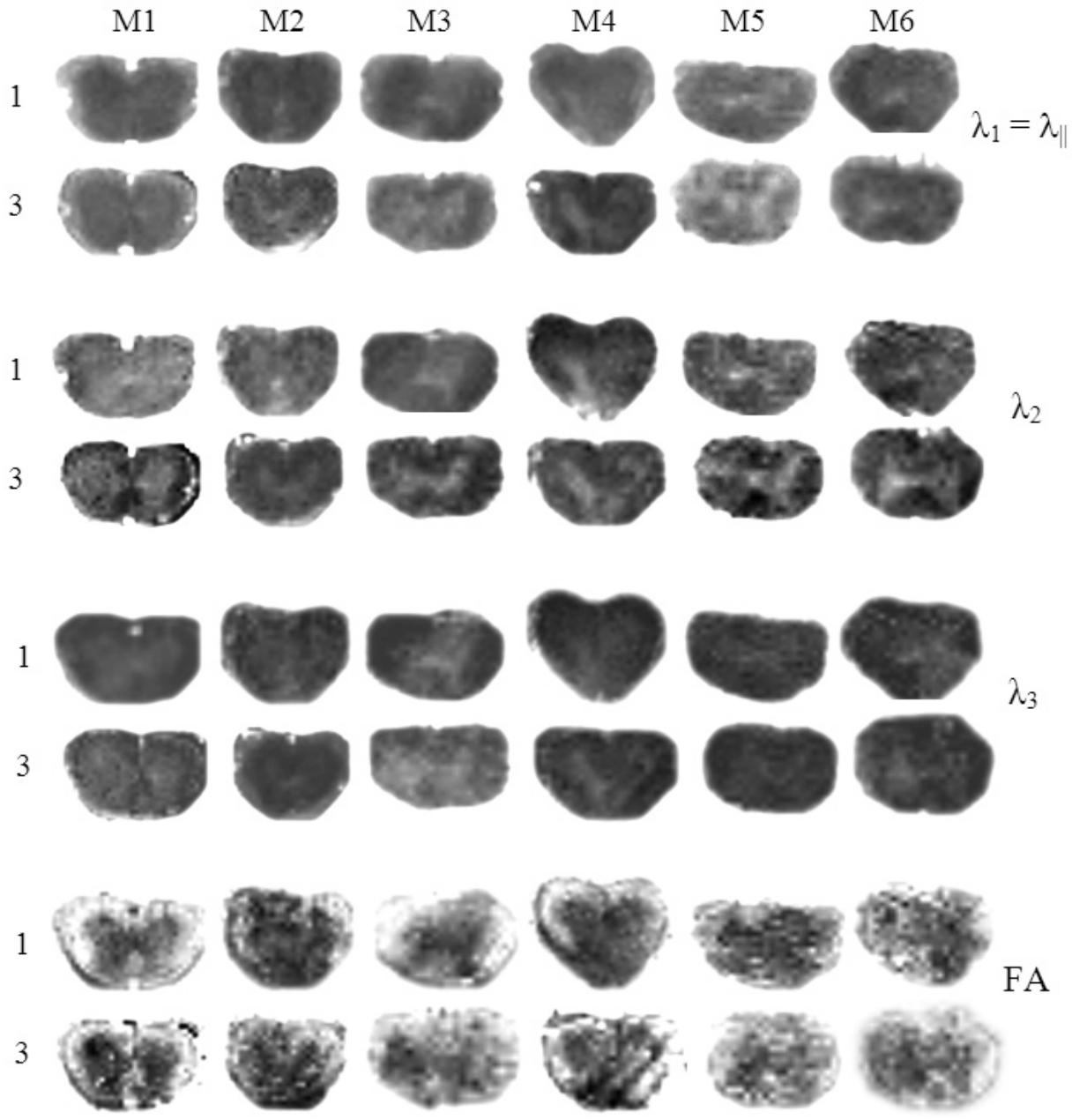

Figure 10. Maps of λ_1, λ_2, λ_3 and FA for all injured spinal cords on postrinjury days 1 and 3.

coil system to achieve an optimal tuning and matching condition as observed in frequency response of the coil impedance. To better evaluate the spatial extent of the lesion, the injured cord was imaged at different planes oriented in transverse and rostral-caudal directions. Figures 5, 6 and 7 present the acquired data from axial and sagittal planes. The images in the figures were organized to delineate the lesions from all animals (M1-M6) and on both postinjury days 1 and 3. The PD images in Figure 5 depict the lesions as they were viewed from the midline in the sagittal plane. The PD and T2 images in Figures 6 and 7 visualize the lesions in axial views at the epicenter, respectively.

Figure 8 compares a sagittal MRI with the images from H&E, PSR and LFB stained histology slides of the injured SC from the mouse M4 in the same sagittal view. The lesion in figure is seen as mainly localized dorsally but expanding along the cord. The MRI reflects a similar pattern of tissue damage and lesion dimension as seen in the histology. Figure 9 provides a similar comparison but in axial view using data from mouse M2.

Figure 10 shows λ_1, λ_2, λ_3 and FA maps computed from diffusion weighted images from the injury epicenter. Perturbations from typical contrast expected from a normal cord for each of these maps reflect microstructural disruptions in the underlying GM and WM tissues. Figure 11 compares changes in $\lambda_{||}$, $\lambda\perp$ and FA measurements

between postrinjury days 1 and 3 within the eight selected ROIs depicted in Figure 2.

Discussion

In the earlier studies of mouse SC with MRI, Wamil et al. [10] employed anatomical images to compare the areas of damage between the injured cords of control and drug treated mouse. Bonny et al. [11] performed structural diffusion-weighted imaging to demonstrate that image contrast changes with the direction of the applied diffusion-sensitizing gradients. Stieltjes et al. [13] used manganese-enhancement to assess neuronal tissue continuity in transected SC. In an ex vivo investigation with female mice, Gaveria et al. [15] studied acute pathological changes at times 2, 4, 8, 16 and 24 hr postinjury in photochemically induced ischemic injuries, and reported the temporal course of alterations in T2 and diffusion properties of injured SC tissue. This study demonstrated the immediate consequences of ischemia and the resulting pathobiology, but it was ex vivo and the photochemical injuries do not account for the mechanical component of damage seen in most human injuries with different secondary outcomes. Loy et al. [18] employed in vivo DTI to evaluate WM of female mice in the hyperacute phase of graded (mild, moderate and severe) SCI at 3 hr postinjury. Kim et al. [17] used DTI on postinjury days 1, 3, 7 and 14 to follow the changes in water diffusion properties in ventrolateral WM of severely injured SCs in live female mice.

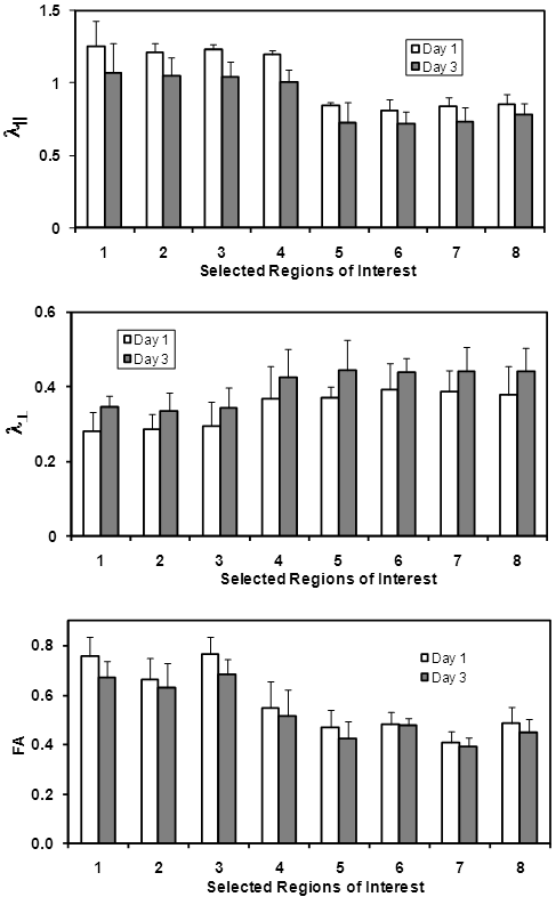

Figure 11. λ_1, λ_2, λ_3 (x10–3 mm²/s) and FA measurements (mean ± Std) within the selected regions of interest in Figure 2.

Our group implemented coil systems (both surface and implantable) to image mouse SC at high resolution and sensitivity [25,29]. In normal live mouse, we measured MR properties and water diffusion characteristics of the cord [12], performed magnetic resonance angiography to visualize the spinal and SC vascularity [14], and developed a method to visualize the corticospinal tract using manganese contrast [16]. In injured mice, we followed the lesion development on postinjury days 1, 7, 14 and 28 using longitudinal MRIs, characterized the behavioral changes and chronic neuropathology using end-point histology [19]. In particular, correlation of the MRI-observed hypointense areas of fibrotic tissue deposition with the gold-standard PSR stained histology was significant.

In this study, we expanded our research focus and investigated mildly injured SC in mouse with a combination of multimodal approaches involving in vivo neuroimaging in conjunction with postmortem tissue analysis in the acute phase of the injury. Several unique aspects, including the gender of mouse employed, injury severity, time points for the measurements and inclusion of the behavioral evaluation, distinguish this work from the previous reports [15-19]. We note that the severity of initial injury as well as the ultimate recovery of motor function after SCI is significantly influenced by gender, being remarkably better in females [30]. In our experimental design, by inducing mild injuries in female mice, the hemorrhage formation was kept to a minimum level and neuronal tissue sparing from the mechanical damage was maximum. Based on our qualitative and quantitative analysis depicted above, we produced sufficient inflammatory mediated neuropathological response in the SC that lead to the loss of neurobehavioral hindlimb function (Figure 4), loss of GM/WM contrast in the anatomical images (Figures 5-7) and microstructural changes in neuronal tissue as detected by the DTI (Figures 10, 11). We confined our studies time-wise into the first 72 hr of the injury, so that mild injuries would not result in significant fibrotic or scar tissue deposition within the injury site. Lack of fibrotic tissue in the injured tissue was confirmed in Figures 8 and 9. Fibrotic tissue in mouse SC produces hypointensity [19]. The signals from these areas would further attenuate with the diffusion weighting. Consequently, DTI analysis with the low signal-to-noise ratio images would not be optimum. Also, wherever it is possible, we presented data from all animals simultaneously. This also allowed us to demonstrate the range of variability in the images or the measured parameters.

Neurobehavioral outcomes. According to Figure 4, the mean score on the first day of the injury read about 4.6. This score reflected that the injured animals were capable of performing distinct functional tasks such as weight support, plantar stepping, or even some forelimb and hindlimb coordination. On day 3, the mean score dropped slightly to about 3.6. This change indicated

slightly worsened hindlimb utilization. Although, the behavioral outcomes were quantitatively described above using BMS, it is also important to point out that the neurological deficits as a result of trauma to the SC may have different origins. Although, mechanically damaged neuronal cell bodies or axons of a contused SC compromise the animal's motor movement, spinal shock also introduces prevalent neurofunctional consequences that affect animal's behavior. While animals under spinal shock may gain full recovery eventually, those with damaged cords demonstrate behavioral deficits that may persist, worsen or improve gradually. Based on these considerations, the behavioral assessments reported above may not be sensitive enough to fully distinguish if the observed deficits are solely due to the condition of spinal shock or physical damage in the acute phase of the injury.

Anatomical MRI. During the preparation for the scan, the mouse was carefully placed supine over an inductively coupled radio frequency coil system to achieve an optimal tuning and matching condition as observed in the frequency response of the coil impedance. This coil system allowed acquiring high quality in vivo data consistently from the injured cords. The lesions were detected by the areas of abnormal intensity patterns localized within the SC parenchyma below the sites of the laminectomy. Overall, the data indicated consistent laminectomies in terms of size and shape and qualitatively depicted similar-looking lesions, demonstrating our capabilities to perform reproducible contusive injuries with our device [24]. The intensity pattern internal to the lesion did not show strong undulations between days 1 day 3 due to the mild nature of the injury. When examined closely, however, the intensity distributions exhibited slight variations spatially between days 1 and 3. This signal behavior was suggestive of lesion experiencing progressive neuropathology.

On day 1, the sagittal images depicted the lesions in mice M1 and M2 by an isotropic hyperintensity. From the changes in the intensity patterns from day 1 to 3, these lesions appeared to enlarge slightly along the cord with time. In contrast, the lesions in the remaining mice (M3-M6) were not as clear on day 1, but became visible on day 3. Each lesion exhibited nearly similar intensity pattern on both PD and T2 images. But, the intensity variation on T2 images had a greater dynamic range with a slight time dependence. The signal features indicated loss of intensity contrast as compared to a normal cord with a butterfly shaped brighter GM in a background of darker WM. This contrast loss was deteriorated further on day 3. Some regions of the WM appeared to be spared especially in the peripheral ring ventral to the cord. The neuronal tissue sparing existed to a lesser degree in the dorsal regions which directly received the impact. Relatively stronger perturbations in the intensity distribution appeared as patchy looking narrow strip of hypointentensity populated centrally within the injured cord. This area was surrounded by large hyperintense, which would otherwise be occupied by GM.

Vascular damage. During the radiological readings of the acquired images in the acute phase of the injury, the areas with hyperintensity were considered to indicate the presence of vasogenic edema and regions with hypointensity represent hemorrhage. Hypointensity was mostly seen in the GM, suggesting damage in its vascular network. These aspects of MRI observed neuropatholy were further explored with the help of histology. H&E stained slides depicted petechial hemorrhage at the injury site, which appeared hypointense on the corresponding PD image (Figures 8 and 9). This was likely to be due to a compromised vascular bed (postcapillary venules or sulcal arterioles) [31]. One aspect of vascular damage is the increased blood spinal cord barrier (BSCB) permeability to the blood constituents. Changes in the BSCB permeability can be detected and quantified using dynamic contrast enhanced MRI performed with the paramagnetic contrast agent Gadalonium [32-34]. The MRI protocol in the current study however did not include this acquisition modality. Therefore, further studies of SCI in mouse with this modality are warranted to understand the vascular response in injured mouse SC.

Scar tissue formation. Fibrotic tissue formation is a feature seen uniquely in the injured mouse SC. PSR stain is sensitive marker for the fibrotic tissue deposition. The image contrast on the PSR stained slides revealed minimal level of scar tissue presence at the injury site by day 3.

Axonal damage and demyelination. The LFB staining confirmed the lesions but with a different contrast sensitive to myelin disruption, enabling the identification of the damaged WM. Away from the injury site, the tissue with intact myelin was seen as confined closer to the surface in an organized fashion within the WM of the cord. The lesions were mostly delineated in the dorsal areas with decreased staining of the demyelinated fibers. The central areas of the lesions were less stained with LFB due to the lack of myelinated axons in the GM.

DTI measurements. The average water diffusion properties of GM and WM in normal mouse SC were reported earlier [12]. The normative baseline values for the parameters λ_1, λ_2, λ_3 (in x 10-3 mm^2/s) and FA are respectively 1.25, 0.71, 0.24 and 0.61 for the GM and 1.95, 0.73, 0.19 and 0.76 for the WM. The differences in diffusion properties of normal SC are mainly due to the cytoarchitecture and orientation of the neuronal tissues in GM and WM. WM appears brighter than GM on λ_1 and FA maps, but WM appears darker than GM in λ_2 and λ_3 maps. In the acute phase of contusion-type SCI, vascular events are more pronounced in GM in the form of microhemorrhages and ischemia while myelin degradation and axonal swelling dictating the neuropathological response in WM. As depicted in Figure 10, deviations in these parameters occur from their normative values as a result of trauma and reflect in the underlying tissue.

According to the data in Figure 11-a, the longitudinal diffusivity $\lambda_{||}$ on day 1 was measured lower than the normative values in both WM and GM of the injured cords. The reduction in $\lambda_{||}$ indicated alterations in the tissue microstructure and associated with cytotoxic edema.

The mean values were about 1.2 x 10-3 mm^2/s in ROIs 1-4 selected within the WM and about 0.8 x 10-3 mm^2/s in the ROIs 5-8 in the GM. On day 3, the trend continued and $\lambda_{||}$ declined further in all of the regions. Kim et al. [17] reported measurements from the ventrolateral WM in severely injured SCs of female mice indicated significant reduction of $\lambda_{||}$ on day 1, as compared to the preinjury levels, and followed by an increase on day 3, indicative of axonal recovery. Our finding of declining $\lambda_{||}$ from day 1 to 3 suggests further deterioration of the WM axons with time rather than recovery. Behavioral scores with slightly declining trend in Figure 4 supports this conclusion. Ex vivo studies with photochemically induced ischemic female mouse SC indicated regionally dependent changes in $\lambda_{||}$ of WM –mostly in dorsal funiculus, to a lesser degree in lateral funiculi and nearly none in ventral funiculus, and no significant variations in GM [15]. Compared to this report, our measurements however indicated no significant regional dependencies for $\lambda_{||}$ in either WM or GM.

The transverse diffusivity ($\lambda\perp$) measurements (Figures 11-b) exhibited an increase for all ROIs 1-8 from day 1 to 3. As shown by the histological data in Figure 9, elevation in $\lambda\perp$ indicated changes in neuronal cell dimensions in transverse directiondue to swelling. The data from GM did not indicate regional variations on either day, but $\lambda\perp$ from the dorsal funiculus - ROI 4 exhibited greater values compared to the other regions (ROIs 1-3) of the WM. This indicated greater axonal swelling in the dorsal WM. It is reasonable to expect that the axons in this region would be the most affected because they directly received the mechanical impact from the contusion. Gaviria et al. [15] reported increased $\lambda\perp$ in the ventral funiculus by 24 hr of ischemic injury. Kim et al. [17] also measured increased $\lambda\perp$ from day 1 to 3 in the ventrolateral WM and demonstrated that this change is due to the axonal damage and myelin loss with histology.

The data in Figure 11-c indicated declining FA values from day 1 to 3, which meant lowered diffusion anisotropy. The measurements from the GM regions were relatively uniform, but those from the WM regions depicted variations. Comparing the FA indices from the four WM regions populated with the ascending sensory and descending motor fiber tracts of the WM, ROI 4 from the dorsal WM was the lowest and ROI 2 from the ventral WM was the second lowest as compared to ROIs 1 and 3. As discussed above, this indicated that the microstructural changes were maximal at the dorsal impact location, but the response was relatively lesser in the ventral WM and the maximum sparing of the axons were in the lateral WM.

Conclusion

The current in vivo MR neuroimaging in conjunction with DTI studies demonstrated that it is possible to gather qualitative and quantitative data from the injured mouse SC with good neurobehavioral and histological correlation. Combining the results together implied that mild-contusion injury in mouse SC produces behavioral deficits and neuropathological response that worsen progressively with time from postinjury day 1 to 3. This suggests that the secondary injury events in this model are actively pursuing and increasingly impairing the neuronal tissue and structure during the first 72 hours. In some experimental studies, the characteristic of slowly progressing injury is sought after because it offers a window of opportunity for therapeutic interventions aimed at altering the course of the lesion development. In this sense, our model has important translational implications. Current preclinical efforts are focused on developing drugs for improving neuroprotection by slowing down the neurodegeneration processes and promoting neuronal recovery. The mild-injury model may be a good candidate to test the efficacy of these drugs in the pipeline. If the goal is to understand the role of specific genes in the repair and recovery of the SC from an injury, then using mild injury model may also be preferable as a test system to chracterize the inflammation response in different stains of "transgenic" or gene "knock out" mice. On the basis of the data produced from these studies, we can conclude that scanning the same animal model with the multimodel MRI protocols provides quantitative measurements that can serve as sensitive and specific in vivo biomarkers for evaluating the neuropathological state of the injured SC and may offer prognostic value for the functional recovery from SCI.

Acknowledgements

This work was funded in part by NIH grants NS052610 and NS054019. The authors thanks Dr. Zhixin L. Huang for helping with MRI scans, Dr. Sorin Craciunas for helping with data analysis, and Dr. Fan Yang for helping with surgeries and histological evaluations.

References

[1] **Guertin PA.** Paraplegic mice are leading to new advances in spinal cord injury research. **Spinal Cord. 2005; 43: 459–461.**

[2] **Rosenzweig ES, McDonald JW.** Rodent models for treatment of spinal cord injury: research trends and progress toward useful repair. **Curr. Opin. Neurol. 2004; 17: 121–131.**

[3] **Steward O, Schauwecker PE, Guth L, Zhang Z, Fujiki M, Inman D, Wrathall J, Kempermann G, Gage FH, Saatman KE, Raghupathi R, McIntosh T.** Genetic approaches to neurotrauma research: opportunities and potential pitfalls of murine models. **Exp. Neurol. 1999; 157: 19–42.**

[4] **Kigerl KA, McGaughy VM, Popovich PG.** Comparative analysis of lesion development and intraspinal inflammation in four strains of mice following spinal contusion injury. **J. Comp. Neurol. 2006; 494: 578–594.**

[5] **Ma M, Wei P, Wei T, Ransohoff RM, Jakeman LB.** Enhanced axonal growth into a spinal cord contusion injury site in a strain of mouse (129X1/SvJ) with a diminished inflammatory response. **J. Comp. Neurol. 2004; 474: 469–486.**

[6] **Bloom FE, Reilly JF, Redwine JM, Wu CC, Young WG, Morrison JH.** Mouse models of human neurodegenerative disorders: requirements for medication development. **Arch. Neurol. 2005; 62: 185–187.**

[7] **Basso DM, Fisher LC, Anderson AJ, Jakeman LB, McTigue DM, Popovich PG.** Basso Mouse Scale for locomotion detects differences in recovery after spinal cord injury in five common mouse strains. **J. Neurotrauma. 2006; 23: 635–659.**

[8] **Inman D, Guth L, Steward O.** Genetic influences on secondary degeneration and wound healing following spinal cord injury in various strains of mice. **J. Comp. Neurol. 2002; 451: 225–235.**

[9] **Sroga JM, Jones TB, Kigerl KA, McGaughy VM, Popovich PG.** Rats and mice exhibit distinct inflammatory reactions after spinal cord injury. **J. Comp. Neurol. 2003; 462: 223–240.**

[10] **Wamil AW, Wamil BD, Hellerqvist CG.** CM101-mediated recovery of walking ability in adult mice paralyzed by spinal cord injury. **Proc. Natl. Acad. Sci. USA. 1998; 95: 13188–13193.**

[11] **Bonny JM, Gaviria M, Donnat JP, Jean B, Privat A, Renou JP.** Nuclear magnetic resonance microimaging of mouse spinal cord in vivo. **Neurobiol. Dis. 2004; 15: 474–482.**

[12] **Bilgen M, Al-Hafez B, Berman NE, Festoff BW.** Magnetic resonance imaging of mouse spinal cord. **Magn. Reson. Med. 2005; 54: 1226–1231.**

[13] **Stieltjes B, Klussmann S, Bock M, Umathum R, Mangalathu J, Letellier E, Rittgen W, Edler L, Krammer PH, Kauczor HU, Martin-Villalba A, Essig M.** Manganese-enhanced magnetic resonance imaging for in vivo assessment of damage and functional improvement following spinal cord injury in mice. **Magn. Reson. Med. 2006; 55: 1124–1131.**

[14] **Bilgen M, Al-Hafez B.** Comparison of spinal vasculature in mouse and rat: investigations using MR angiography. **Neuroanatomy. 2006; 5: 12–18.**

[15] **Gaviria M, Bonny JM, Haton H, Jean B, Teigell M, Renou JP, Privat A.** Time course of acute phase in mouse spinal cord injury monitored by ex vivo quantitative MRI. **Neurobiol. Dis. 2006; 22: 694–701.**

[16] **Huang ZL, He YY, Bilgen M.** In vivo tracing of corticospinal tract in mouse using manganese-enhanced contrast. **J. Neurol. Sci. [Turk]. 2007; 24: 38–44.**

[17] **Kim JH, Loy DN, Liang HF, Trinkaus K, Schmidt RE, Song SK.** Noninvasive diffusion tensor imaging of evolving white matter pathology in a mouse model of acute spinal cord injury. **Magn. Reson. Med. 2007; 58: 253–260.**

[18] **Loy DN, Kim JH, Xie M, Schmidt RE, Trinkaus K, Song SK.** Diffusion tensor imaging predicts hyperacute spinal cord injury severity. **J. Neurotrauma. 2007; 24: 979–990.**

[19] **Bilgen M, Al-Hafez B, Alrefae T, He YY, Smirnova IV, Aldur MM, Festoff BW.** Longitudinal magnetic resonance imaging of spinal cord injury in mouse: changes in signal patterns associated with the inflammatory response. **Magn. Reson. Imaging. 2007; 25: 857–864.**

[20] **Aimone JB, Leasure JL, Perreau VM, Thallmair M.** Spatial and temporal gene expression profiling of the contused rat spinal cord. **Exp. Neurol. 2004; 189: 204–221.**

[21] **Ousman SS, David S.** MIP-1alpha, MCP-1, GM-CSF, and TNF-alpha control the immune cell response that mediates rapid phagocytosis of myelin from the adult mouse spinal cord. **J. Neurosci. 2001; 21: 4649–4656.**

[22] **Parker D.** Pharmacological approaches to functional recovery after spinal injury. **Curr. Drug Targets CNS Neurol. Disord. 2005; 4: 195–210.**

[23] **Pearse DD, Bunge MB.** Designing cell- and gene-based regeneration strategies to repair the injured spinal cord. **J. Neurotrauma. 2006; 23: 437–452.**

[24] **Bilgen M.** A new device for experimental modeling of central nervous system injuries. **Neurorehabil. Neural. Repair. 2005; 19: 219–226.**

[25] **Bilgen M.** Simple, low-cost multipurpose RF coil for MR microscopy at 9.4 T. **Magn. Reson. Med. 2004; 52: 937–940.**

[26] **Bilgen M.** Imaging corticospinal tract connectivity in injured rat spinal cord using manganese-enhanced MRI. **BMC Medical Imaging. 2006; 6: 15.**

[27] **Bilgen M, Elshafiey I, Narayana PA.** Mohr diagram representation of anisotropic diffusion tensor in MRI. **Magn. Reson. Med. 2002; 47: 823–827.**

[28] **Bilgen M, Narayana PA.** Mohr diagram interpretation of anisotropic diffusion indices in MRI. **Magn. Reson. Imaging. 2003; 21: 587–572.**

[29] **Bilgen M.** Magnetic resonance microscopy of spinal cord injury in mouse using a miniaturized implantable RF coil. **J. Neurosci. Methods. 2007; 159: 93–97.**

[30] **Farooque M, Suo Z, Arnold PM, Wulser MJ, Chou CT, Vancura RW, Fowler S, Festoff BW.** Gender-related differences in recovery of locomotor function after spinal cord injury in mice. **Spinal Cord. 2006; 44: 182–187.**

[31] **Noble LJ, Donovan F, Igarashi T, Goussev S, Werb Z.** Matrix metalloproteinases limit functional recovery after spinal cord injury by modulation of early vascular events. **J. Neurosci. 2002; 22: 7526–7535.**

[32] **Bilgen M, Narayana PA.** A pharmacokinetic model for quantitative evaluation of spinal cord injury with dynamic contrast-enhanced magnetic resonance imaging. **Magn. Reson. Med. 2001; 46: 1099–1106.**

[33] **Bilgen M, Abbe R, Narayana PA.** Dynamic contrast-enhanced MRI of experimental spinal cord injury: in vivo serial studies. **Magn. Reson. Med. 2001; 45: 614–622.**

[34] **Bilgen M, Dogan B, Narayana P.** In vivo assessment of blood-spinal cord barrier permeability: serial dynamic contrast enhanced MRI of spinal cord injury. **Magn. Reson. Imaging. 2002; 20: 337.**